Microstructuring Process in Oleogels Formulated with Vegetable Oils and Monoglycerides: A Comparison of Non-Isothermal Nucleation Kinetics by Spectrophotometric and DSC Analysis

Javier Isaac Contreras-Ramírez¹, Esperanza Acosta-Gurrola¹, Walfred Rosas-Flores¹, Jose Alberto Gallegos-Infante², and Jorge Toro-Vazquez³

¹Instituto Tecnológico de Durango ²TecNM/Instituto Tecnologico de Durango ³Universidad Autonoma de San Luis Potosi

June 28, 2022

Abstract

The initial oleogelation process (microstructuring) as well as the formulation are determinant to obtain the desired characteristics in oleogels with potential application in the industry. The microstructuring process in oleogels has been extensively studied by means of techniques highly sensitive to thermal variations, such as differential scanning calorimetry (DSC). However, there are other readily available techniques and equipment that can be employed to perform similar evaluations. Non-isothermal nucleation kinetics by spectrophotometric methods can be used as alternatives to basic crystallization studies in oleogels. Therefore, in this research a comparison of both techniques is presented, highlighting their similarities, advantages and limitations, in the study of the microstructure of oleogels. Oleogels were obtained with a minimum concentration of gelator and another saturated one, using vegetable oils of different degrees of saturation. The crystallization profiles of the oleogels were obtained by DSC, a non-isothermal nucleation kinetics was performed from the molten system and the final microstructure was evaluated by optical microscopy. The Fisher-Turnbull and Avrami model was used to evaluate the behavior during microstructuring. A gap was observed during the crystallization process by DSC which can be evaluated by spectrophotometry. Differences in the microstructuring process were found in both methods due to the temperature ramp used and formulation variables. The results obtained by spectrophotometry indicate that it can be a good alternative, easily accessible in oleogel crystallization studies, when high sensitivity or very specific thermal parameters are not required.

INTRODUCTION

Oleogels have proved to be an important alternative for the replacement of hydrogenated fat in food matrices in recent years, as well as vehicles with good stability in the release of nutraceuticals (Puşcaş et al., 2020). The positive impact on improving the nutritional and health profile as well as some other applications have already been addressed and discussed extensively (Alvarez et al., 2021). Oleogels can be defined as "pseudoplastic" and thermoreversible semi-solid systems composed of a liquid phase (organic solvent) that is immobilized by a three-dimensional network formed from the self-assembly of gelling molecules (Zeng et al., 2021). The three-dimensional network in physical oleogels is formed by supramolecular self-assembly that is governed by non-covalent interactions such as hydrogen bonds, π - π stacking, Van der Waals interactions, and electrostatic interactions. Obtaining oleogels with low molecular weight molecules, such as monoglycerides, and governed by the aforementioned interactions, are known as physical gels. The obtaining of oleogels starts by solubilizing the gelling agent in a heated organic solvent, so that once the maximum solubility of gelling agent-solvent is exceeded, the system is cooled to a temperature below the solubility limit (Krafft temperature). This starts a reorganization of the gelling molecules leading to a nucleation process (Li & Liu, 2010). Once nucleation occurs in the oleogels, a process of crystallization and growth of structures by the gelling agent begins. This process resembles the crystallization of fat (Bayés-García et al., 2015). The crystalline structures that develop from the newly formed nuclei arise from a series of dimensionality patterns and crystal growth geometry. Transition temperatures, gelation and final properties of oleogels depend not only on the nature of the organic solvent and gelling agent, but also on the cooling rate and storage conditions, i.e., they depend on different thermal and kinetic parameters (Ashkar et al., 2019). Nucleation and dimensionality parameters of crystal growth during oleogelation are important factors in determining the microstructure and crystallinity properties in oleogels. The initial crystallization (microstructuring) process of oleogels can be studied from a fully melted system by minitoring their thermal and kinetic properties during crystallization, as well as the resulting microstructure. This crystallization process is currently evaluated at the macroscopic level by thermal techniques such as differential scanning calorimetry (DSC), which allows to obtain clear crystallization profiles of oleogels (Puşcaş et al., 2021). Microstructure on the other hand can be evaluated by almost any microscopy equipment that allows the identification of crystalline structures. However, the use of this highly efficient and most common equipment in laboratories studying oleogel systems focuses mainly on the crystallization process and the final crystal structure. This leaves the initial stage of the microstructuring process "nucleation" unable addressed during the characterization of new oleogel systems. However, spectrophotometric techniques give the possibility to obtain an absorbance response proportional to the solute concentration and solid formation.

The Avrami equation is used to model crystallization kinetics under isothermal conditions, however, it can be accommodated within non-isothermal evaluations (Rogers & Marangoni, 2009). Experimental reality limits the rate at which a system reaches a set crystallization temperature, and at the industrial level in the development of edible fat products, crystallization takes place under non-isothermal conditions. These conditions imply having considerations on the cooling rate that have already been well addressed by Marangoni et al. (2017), The Lambert-Beer law states that the absorbance is directly related to the intrinsic properties of the analyte, to its concentration and to the path length of the radiation beam as it passes through the sample. Toro-Vázquez et al. (2000), indicate that the birefringence of the oleogel crystals can influence the results obtained by spectrophotometry in comparison with those obtained by DSC. This is because heterogeneous, sporadic nucleation and secondary crystallization are more as time progresses, so the amount of crystals is not constant with time. Therefore, the starting point of "microstructuring" could be studied by non-isothermal nucleation kinetics by spectrophotometry, which is outside the limits of DSC. This would allow a broader perspective of the oleogelation process. Therefore, the objective of the present work was to perform a comparison in the study of the initial microstructuring process of oleogels, using non-isothermal nucleation kinetics by spectrophotometry versus a DSC analysis. Identifying the scopes and limitations of the different techniques.

MATERIALS AND METHODS

Vegetal Oils and Monoglyceride Analysis

Commercial canola (CA) and coconut (CN) oils were used, purchased at a local supermarket (Durango, Mexico), the gelling agent Myverol (MY) 18-04PK (monoglyceride mixture) was kindly provided by Kerry, SW Food Technology (Nuevo Leon, Mexico). The oil and MY samples were analyzed for fatty acid (FA) profile by gas chromatography (GC). GC analysis was performed on a GC-2010 Shimadzu (Shimadzu Corp., Kyoto, Japan) with a Varian CP 7420 column. The official methods established by AOCS Ce 2-66 and Ce 1h-05 (AOCS, 2017) were followed.

Determination of the Minimal Gelling Concentration and Obtaining Oleogels

Solutions of MY were prepared in CA and CN at 0.5% w/w intervals up to a concentration of 3% w/w. The solutions were heated separately and homogenized by magnetic stirring (80°C, 100rpm, 10min). The solutions were stored in 20 mL glass vials (28 mm inner diameter, 57 mm height) at 20°C under controlled conditions for 24h. The minimum gelation concentration (MGC) in each oil was determined as the lowest MY concentration at which no flow was observed after inverting the vials for 1h at room temperature (20°C)

(Aguilar-Zárate et al., 2019). Oleogels (OGs) were prepared with the MGC and with 4 times the MGC value to obtain saturated systems (SAT). The OGs were obtained by separately heating the different oils with the MGC and SAT concentrations of MY and homogenizing as mentioned above. The OGs were stored for 24h at 20°C under controlled conditions.

Thermal Evaluation

Crystallization and melting profiles of CA, CN and MY were obtained with a DSC Q-2000 differential scanning calorimeter (TA Instruments, New Castle, DE, USA) equipped with a cooling unit. The DSC equipment was calibrated with indium. The samples (4-7mg) were hermetically sealed in aluminum capsules. For the individual components (CA, CN and MY) a fully melted sample (100°C) was started, a cooling ramp was performed to -70°C (3°C/min), and then a second heating was performed to 80°C (3°C/min). For the OGs, a first heating (thermal memory erase) from storage temperature (20°C) to 80°C (10°C/min) was performed, this from the thermal results of individual components. This was followed by a cooling down to 0°C (3°C/min). The temperatures and enthalpies corresponding to the exotherms were determined with Universal Analysis 2000 Ver. 4.5A software (TA Instruments-Waters LLC).

Non-isothermal Nucleation Kinetics

Non-isothermal nucleation kinetics of OGs were obtained on a Jenway 6705 spectrophotometer (OSA, UK), coupled to a water bath with Techian temperature controller (OSA, UK). Kinetics were performed from OGs melted at 80°C (isothermal 10 min) and then cooled to room temperature. During absorbance kinetics, readings were taken every 10s (550 nm) (Garcia-Andrade et al., 2020). Nucleation induction time (t_n) , nucleation rate (J) and nucleation free energy (ΔG_n) were determined using the Fischer-Turnbull model (Rogers & Marangoni, 2009), described below:

$$J = \frac{1}{t_n} \ (1)$$

The cooling rate (\emptyset) was also determined as a ratio of temperature change over time (simulating the DSC cooling ramp):

 $O = \Delta T$

greekt (2)

The effective supercooling (δ) , which incorporates a thermodynamic component from an initial temperature (80°C) where the material is completely melted, to the nucleation process (Ti-T_n) and a kinetic component (\emptyset) , was determined:

$$\delta = \Delta T_{c}$$

 $english\sqrt{2O}$ (3)

The determination of $\Delta\Gamma_{\nu}$ was determined from the kinetic parameters obtained above:

$$\Delta\Gamma_n = \frac{\mathrm{mk}\delta}{(\Delta T)^2} (4)$$

where m is the slope of the ratio of δ and the normalized nucleation rate (J/Jmax) and k is the Boltzman constant.

Avrami Model

The Johnson-Mehl-Avrami equation (eq. 5) was used to model the spectrophotometric data for nonisothermal nucleation kinetics (Garcia-Andrade et al., 2020):

$$ln(1-F) = -zt^n (5)$$

where n is the Avrami exponent, z is a constant associated with the overall phase transition velocity, t is the time and F is the uncrystallized fraction over time. Integer values (1, 2, 3) of n represent the formation of rod-shaped crystals (1-D), disk-shaped crystals (2-D) and spherical crystals (3-D), respectively. A noninteger value indicates the formation of irregularly shaped crystals. The methodology of Toro-Vázquez et al. (2000) was followed to calculate the Avrami parameters from the exotherms obtained by DSC. F values were taken as the integration of the non-isothermal crystallization curves. The n and z parameters were determined by nonlinear estimation using the Rosenbrock and Quasi-Newton algorithm.

Polarized Light Microscopy

Micrographs of OGs were obtained on an Axio-Lab A.1 polarized light filter optical microscope (Zeiss, Jena, Germany) equipped with an Axio-Cam ERc 5S digital camera. The image set was processed with ZEN 2.3 lite software (Blue edition, Zeiss, Jena, Germany). From the obtained micrographs, a grayscale image analysis was performed by the FDim software of Martin Reuter (MIT-Cambridge, MA, USA) to obtain the fractal dimension (FD) values, where the best FD value was selected according to the obtained correlation coefficients.

Stadistical Analysis

Analysis of variance (ANOVA), and comparison of means by Fisher (P < 0.05) were performed. Statistical analysis and nonlinear estimations were performed with Statistica, v 12.5 software (StatSoft, OK, 2014).

RESULTS AND DISCUSSION

MGC and SAT of OGs

Table 1 shows the results of fatty acid composition of vegetable oils and monoglycerides obtained by GC. The difference in the composition of saturated (SFA), monounsaturated (MFA) and polyunsaturated (PFA) fatty acids was observed in both oils and MY. CA was found to be rich mostly in medium-chain MFA and PFA (66.28 and 27.78%), while CN is mainly composed of short-chain SFA (90.82%). FA composition for these oils is similar to that reported by other authors (Garcia-Andrade et al., 2020), however, the FA profile of MY was different from that reported by Giacomozzi et al. (2021), (C16:0 43.91 \pm 0.07% and C18:0 53.65 \pm 0.07%). Even being the gelling agent Myverol, the product used for this investigation had a higher percentage of C16:0 (palmitate, 58.72 \pm 0.10%) and lower percentage of C18:0 (stearate 39.67 \pm 0.11%). However, it is possible that the degree of saturation of the oils affected the properties of the oleogel.

The MGC of MY at room temperature was different for each type of oil (CA = 2.5% w/w, CN = 2% w/w) (Fig. 1), this due to differences in their chemical composition (Table 1), where a composition mostly saturated in CN allows MY to retain the liquid phase more easily. However, for comparative purposes, we continued with 2.5% w/w MY in both oils in the following evaluations. It is possible that using a lower storage temperature may require a lower amount of gelator due to reduced intermolecular Brownian motion, however, a lower temperature also promotes sub- α crystallization, and consequently there is a greater likelihood of early polymorphism (Lopez-Martinez et al., 2014). The MGC values found in this work for CA and CN are lower than those reported by other authors for oils with high triolein content using a commercial monoglyceride ($^{3.5\%}$ w/w) (Aguilar-Zárate et al., 2019). It is known that this concentration depends on the solubility of the gelling agent in the vegetable oil, as well as the cooling rate and temperature. However, the solubility is closely linked to the solvent composition. In addition, a higher concentration of gelant results in lower solubility, which allows greater molecule-molecule interaction of the gelant, promoting self-assembly and having higher oil retention capacity.

Crystallization and Melting Profiles

The thermograms of the vegetable oils and MY are shown in Figure 2. The temperatures of the different exotherms and endotherms of each component were determined. CA presented a crystallization and melting temperature at $-55.66\pm0.17^{\circ}$ C and $-18.91\pm0.12^{\circ}$ C, respectively. CN presented two crystallization signals, one $-3.11\pm0.27^{\circ}$ C and the other at $7.26\pm0.29^{\circ}$ C, this probably due to the composition of triglycerides in CN, which are formed by a lower percentage of PFA that crystallize at lower temperature (Table 1). The melting temperature of CN was at $23.08\pm0.13^{\circ}$ C (Ghosh & Rousseau, 2009). Two exotherms were observed

in MY, one from the lamellar state crystallization Λa (63.58±0.03°C) and one from the solid-solid transition $\Lambda a = \Sigma v \beta$ -a (11.47±0.16°C). Correspondingly, during heating, Sub- $\alpha = L\alpha$ (12.93±0.15°C) and melting Λa (65.52±0.13°C) temperatures were identified. These values are similar to those reported by other authors for commercial monoglycerides, where polymorphic states were identified by X-ray diffraction (López-Martínez et al., 2014). According to some authors (Vereecken et al., 2009), by employing pure compounds individually, the main components of MY have different crystallization and melting points, however, possessing a similar structure palmitic (C16:0) and stearic (C18:0) acid, they can generate a mixed L α crystallization (López-Martínez et al., 2014), so the proportion in which these are found in Myverol gelator can result in differences in thermal and microstructural properties.

Since MY is the component responsible for gel structuring and formation, an analysis of the changes that its endotherms can present in oleogels with formulation and concentration variables was performed. Changes in the crystallization of Aa were monitored (Fig. 3). In oleogels with MGC it was possible to find MY TC values at $31.30\pm0.10^{\circ}$ C in CA and $28.96\pm0.19^{\circ}$ C in CN (Table 2), these values are very similar to those reported by other authors, in a mixture used of commercial monoglyceride with lecithin (Aguilar-Zárate et al., 2019). However, unlike the exotherm with two peak maxima reported by Aguilar-Zárate et al. (2019), in these systems a single peak maximum is observed, albeit in a more robust exotherm. While these differences may be due to the temperature ramp, it is also due to the difference in the proportions of palmitic and stearic acid. Similarly, a single exotherm was found in the SAT systems (Fig. 3). However, the crystallization of Aa was at a higher temperature ~49°C (Table 2).

Non-Isothermal Nucleation

In the development of the non-isothermal nucleation kinetics by spectrophotometry, the values of T_{CS} , T_{CO} and T_C , as well as the cooling ramp used in DSC, were taken as a starting point. Figure 4 shows the kinetics obtained for each system. It can be observed that there is a higher absorbance response in the systems with higher MY concentration (SAT), this as a response to the higher formation of MY crystals (solid fraction). It was also observed that there is a higher absorbance response in CN systems compared to CA. The nucleation kinetics initially present a time interval where the system is completely melted (baseline), followed by an almost exponential growth. The point where the increase from the baseline starts is the beginning of nucleation (García-Andrade et al., 2020). Subsequently, the absorbance values present an almost constant trend (Fig. 4). However, it was found that for the CN_{MGC} system there is a second increase after this usual trend. This was not observed in CN_{SAT} because the high concentration of MY in conjunction with the nature of CN gives higher absorbance values in response, which overlies the second increase. This second increase in absorbance values in the CN_{MGC} system corresponds to the crystallization of the oil, which although it has a high crystallization point, it is at a lower temperature than the crystallization of MY (Fig. 2).

From the graphs shown it was possible to determine the most relevant kinetic and thermal parameters during nucleation (Table 3). Shorter nucleation times were obtained in SAT systems compared to MGC, and consequently, higher nucleation rates (J) were obtained. No significant differences were found between the oil variable with high MY concentrations, however, at MGC, the shortest tn was for CN. Shorter nucleation times have been reported with the use of saturated oils, in systems with high concentrations of structurants (Garcia-Andrade et al., 2020), so it was necessary to evaluate the effect of concentration additionally. The differences observed by oil type in MGC systems may be due to the unsaturation of the oils, and the content of free fatty acids (FFA), since FFA require lower activation energy in the crystallization process with respect to TAGs. These compositional differences may be more representative in systems with low gelator concentrations. Due to the inverse correlation between t_n and T_n , higher values of T_n and lower values of δ were obtained at shorter times, indicating that a lower thermodynamic inductive force is needed in oleogels with higher MY concentration.

The response exhibited by SAT systems is mainly due to a higher amount of attraction and hydrogen bonding interactions of the amphiphilic molecule with the TAGs of the oil. A higher amount of hydrogen bonds promotes a faster orientation of the polar moiety of the MY by aligning its hydrocarbon chains (attractive and hydrophobic interactions) and generating a faster first solid core (Contreras-Ramírez et al., 2021). Regarding the $\Delta\Gamma_{\nu}$ values, the values closest to equilibrium were obtained in the SAT systems. Except for the $\Delta\Gamma_{\nu}$ values that were smaller with CN oil, no significant differences were found by oil type at SAT concentrations. This is due to a higher interaction of SFA content and high MY concentration.

Avrami Parameters

Table 4 shows the parameters obtained with the Avrami model for the different oleogels ($\mathbb{R}^2 > 0.9$). It was found that all the systems present a linear growth (1-2) according to the values of n, with a onedimensional growth geometry (Toro-Vázquez et al., 2000). A non-integer value indicates the formation of irregularly shaped crystals. This aforementioned growth is characteristic of fibrillar-type structures found in monoglyceride systems. Fractional values have already been explained in other investigations where they are attributed to the formation of structures from different types of nuclei (heterogeneous nucleation) (García-Andrade et al., 2020). It was found that values of ngreater than 1 correspond to systems with lower MY concentration (Table 4). This can be understood by taking into consideration what was observed in Table 3, where oleogels with lower MY content showed longer nucleation times and consequently slower growth or branching times (z). A slower growth rate allows an almost two-dimensional growth due to a greater distance between the already formed nuclei and the freedom they present in the transfer of energy and interaction to form such structures. The concentration of structuring agents is a determining factor for the growth rate in oleogel systems.

Figure 5 shows the time evolution of the crystalline mass (F \times 100), for different MY concentrations in CA and CN oleogels. The curves followed the same general sigmoidal trend of behavior, with a time difference of [?]4min, the crystallization rate increased beyond the T_{CS} value until reaching zero crystallization rate at F x 100 = 100. The times where the increase from the baseline is presented corresponded to the T_{CS} values shown in Table 2. The times obtained by DSC ($t_{SC}^{-T}T_{SC}$) (CA_{MGC}=14.52min, CA_{SAT}=10.31min, $CN_{MGC} = 14.24$ min and $CN_{SAT} = 10.07$ min) were similar to those obtained by spectrophotometry (t_n) and also to that reported in rheological analyses of the cooling process (Palla et al., 2019). However in the spectrophotometry graph (Fig. 4) it can be observed that there is an increase in absorbance during the 60min, while in by DSC (Fig. 5) a maximum of crystallization is reached in less time. This is due to two situations, the first is that in the spectrophotometry kinetics when reaching the ambient temperature ([?]20degC), the programming was set so that the temperature remained constant due to the limitations of the equipment. This execution, together with the temperature differential generated between the spectrophotometer chamber and the recirculating water bath, resulted in a slower (almost isothermal) crystallization in the final stage of the experiment. In the DSC evaluation, it was possible to reach 0 degC by maintaining a constant cooling rate and a fixed TSTOP for each exotherm. It should also be noted that very low regression coefficients $(R^2_{i0}, 70)$ were obtained in obtaining the values of z and n by DSC. These R^2 values are low compared to those obtained by Toro-Vázquez et al. (2000),. However, it should be noted that the analysis developed by them was under isothermal conditions (Toro-Vázquez et al., 2000), while in this work, non-isothermal conditions were used, which results in obtaining less symmetrical exotherms and an irregular distribution of the crystalline fraction. However, the values of the initial temperature versus nucleation temperature allow us to detect a range of temperatures where there is an initial crystallization process (nucleation) that could be omitted by conventional DSC. Therefore, nucleation kinetics from spectrophotometry is a good alternative to study the initial stage of microstructuring in OGs, which by DSC is not persived.

Microstructure

Micrographs were obtained with a polarized light filter (10X objective), where the birefringence of the structures formed by the MY is present (Fig. 6). More crystalline structures were found in the SAT systems. This is due to the fact that a higher concentration of MY provides more nucleation points from which the formation of fibrillar crystalline structures occurs, which in turn form the three-dimensional network that immobilizes the liquid oil. Gelator saturation in SAT systems affects the crystalline units in oleogels, this can trigger a decrease in their structural integrity in the initial crystallization process, due to the increased nucleation-crystallization rate, resulting in lower nvalues due to the formation of individual crystal lattices

(Table 4). This can be understood as a constraint on network structuring, since individual networks will exhibit less bonding between their structures in the long term. The nucleation rate is closely related to the number of structural elements in an oleogel.

In Figure 6, a higher degree of structuring is observed in CN systems, because the presence of MY promotes early crystallization of the oil at ambient temperature, even at low concentrations (MGC). A better distribution of crystalline structures throughout the plane can be beneficial to obtain desired solid properties, however, an oversaturation of the same can also result in a high hardness and brittle system. From an image analysis, fractal dimensionality values were determined by the correlation method (FD) with high R^2 values (Table 4). Fractal dimensionality is an index that points out the crystalline mass distribution in the lattice of an oleogel. All systems present [?]2 values, it is worth mentioning that the geometry of a growing crystal is not determinant of its dimensionality due to the fact that nucleation can be homogeneous or heterogeneous. The DF values reported here are lower than those reported by Palla et al. (2019), with a saturated monoglyceride concentration in a high oleic oil. Differences can be found between the Avrami and FD values of n (Table 4). The geometrical growth of a crystalline structure, in turn, is not independent of the MY concentration, since a higher concentration of gelator in a mostly saturated solvent promotes heterogeneous crystallization from the first structures formed also inducing the sporadic generation of new nucle.

Conclusions

In conclusion, non-isothermal nucleation kinetics by spectrophotometry allow to evaluate the initial stage of oleogel microstructuring, even before it is perceived in the DSC technique. Non-isothermal nucleation kinetics are a good method to study crystallization processes that do not require thermal high precision or specific thermal parameters. The degree of saturation of the oils and high concentrations of gelling agent play an important role in nucleation, due to a higher gelling agent-oil interaction, which can influence the supramolecular organization and thus the final microstructural properties of the oleogels.

ACKNOWLEDGEMENTS

The first author gratefully acknowledges the doctoral studies grant (Grant No. 607796) from CONACyT (Consejo Nacional de Ciencia y Tecnologia) of Mexico. Technology) of Mexico, and the institutional support for a national technical research stay granted by COCyTED (Consejo de Ciencia y Tecnologia del Estado de Durango) is also gratefully acknowledged.

CONFLICT OF INTEREST

The authors declare that they have no conflict of interest.

AUTHORSHIP

Javier Isaac Contreras-Ramirez: Data acquisition and wrote the first draft of the manuscript. Esperanza Acosta-Gurrola: Data acquisition and analysis. Walfred Rosas-Flores: Data analysis. Jose Alberto Gallegos-Infante: Data analysis and interpretation.Jorge Fernando Toro-Vazquez: Data analysis and conception.

ETHICAL STATEMENT

This research falls outside of human or animal studies and institutional ethical approval was not required.

ORCID

Javier Isaac Contreras-Ramirezhttps://orcid.org/0000-0002-4408-052X

References

Puşcaş A, Mureşan V, Socaciu C, Muste S. Oleogels in Food: A Review of Current and Potential Applications. Foods. 2020;9:70-98.doi:10.3390/foods9010070 Alvarez MD, Cofrades S, Espert M, Sanz T, Salvador A. Development of Chocolates with Improved Lipid Profile by Replacing Cocoa Butter with an Oleogel. Gels. 2021;7:20. doi:10.3390/gels7040220

Zeng L, Lin X, Li P, Liu F-Q, Guo H, Li H-H. Recent advances of organogels: from fabrications and functions to applications. Prog Org Coat. 2021;159:106417. doi:10.1016/j.porgcoat.2021.106417

Li J-L, Liu X-Y. Architecture of Supramolecular Soft Functional Materials: From Understanding to Micro-/Nanoscale Engineering. Adv Funct Mater. 2010;20:3196–3216. doi:10.1002/adfm.201000744

Bayés-García L, Patel AR, Dewettinck K, Rousseau D, Sato K, Ueno S. Lipid crystallization kinetics — roles of external factors influencing functionality of end products. Curr Opin Food Sci. 2015;4:32-38.doi:10.1016/j.cofs.2015.04.005

Ashkar A, Laufer S, Rosen-Kligvasser J, Lesmes U, Davidovich-Pinhas M. Impact of different oil gelators and oleogelation mechanisms on digestive lipolysis of canola oil oleogels. Food Hydrocoll. 2019;97:105218.doi:10.1016/j.foodhyd.2019.105218

Puşcaş A, Mureşan V, Muste S. Application of Analytical Methods for the Comprehensive Analysis of Oleogels—A Review. Polymers. 2021;13:1934-1958.doi:10.3390/polym13121934

Rogers MA, Marangoni AG. Solvent-Modulated Nucleation and Crystallization Kinetics of 12-Hydroxystearic Acid: A Nonisothermal Approach. Langmuir. 2009;25:8556-8566. doi:10.1021/la8035665

Marangoni AG. Non-isothermal Nucleation Kinetics in Fats. In: Marangoni AG. Kinetic Analysis of Food Systems. Springer, Cham. 2017. p. 145-160.doi:10.1007/978-3-319-51292-1_9

Toro-Vázquez JF, Briceño-Montelongo M, Dibildox-Alvarado E, Charó-Alonso M, Reyes-Hernánez J. Crystallization Kinetics of Palm Stearin in Blends with Sesame Seed Oil. J Am Oil Chem Soc. 2000;77:297-310.doi:10.1007/s11746-000-0049-x

AOCS Official Methods Ce 1h-05 and Ce 2-66 Reapproved 2017, Official Methods and Recommended Practices of the AOCS 7th Ed. (American Oil Chemists' Society, Urbana, IL. USA, 2017)

Aguilar-Zárate M, De la Peña-Gil A, Álvarez-Mitre FM, Charó-Alonso MA, Toro-Vázquez JF. Vegetable and Mineral Oil Organogels Based on Monoglyceride and Lecithin Mixtures. Food Biophys. 2019;14:326-345. doi:10.1007/s11483-019-09583-1

García-Andrade M, González-Laredo RF, Rocha-Guzmán NE, Rosas-Flores W, Moreno-Jiménez MR, Peña-Ramos EA, Gallegos-Infante JA. Influence of ethyl cellulose in a multicomponent mixture (sorbitan monopalmitate-vegetable oils) on physicochemical properties of organogels. Rev Mex Ing Quim. 2020;19:953-968. doi:10.24275/rmiq/Alim801

Giacomozzi AS, Carrín ME, Palla CA. Storage Stability of Oleogels Made from Monoglycerides and High Oleic Sunflower Oil. Food Biophys. 2021;16:306-316. doi:10.1007/s11483-020-09661-9

López-Martínez A, Morales-Rueda JA, Dibildox-Alvarado E, Charó-Alonso MA, Marangoni AG, Toro-Vázquez JF. Comparing the crystallization and rheological behavior of organogels developed by pure and commercial monoglycerides in vegetable oil. Food Res Int. 2014;64:946–957.doi:10.1016/j.foodres.2014.08.029

Ghosh S, Rousseau D. Freeze-thaw stability of water-in-oil emulsions. J Colloid Interface Sci. 2009;339:91–102. doi:10.1016/j.jcis.2009.07.047

Vereecken J, Meeussen W, Foubert I, Lesaffer A, Wouters J, Dewettinck K. Comparing the crystallization and polymorphic behaviour of saturated and unsaturated monoglycerides. Food Res. Int. 2009;42:1415-1425.doi:10.1016/j.foodres.2009.07.006

Contreras-Ramírez JI, Villanueva-Fierro I, González-Laredo RF, Toro-Vázquez JF, Pérez-Martínez JD, Rosas-Flores W, Gallegos-Infante JA. Study of the relationship of hydrogen bonding and hydrophobic

interactions in W/O organogel emulsions by Raman microspectroscopy. Colloids Interface Sci Commun. 2021;44:100486.doi:10.1016/j.colcom.2021.100486

Palla C, de Vicente J, Carrín ME, Gálvez-Ruiz MJ. Effects of cooling temperature profiles on the monoglycerides oleogel properties: A rheo-microscopy study. Food Res Int. 2019;125:108613.doi:10.1016/j.foodres.2019.108613

FIGURE LEGENDS

Fig. 1 Photograph of inverted vials with different MY concentration

Fig. 2 Vegetable oils and Myverol thermograms

Fig. 3 MY crystallization in CA and CN oleogels

Fig. 4 Non-isothermal nucleation kinetics of CA and CN oleogels with different MY concentration

Fig. 5 Percentage of reduced crystallinity (F \times 100) as a function of time in CA and CN oleogels at different MY concentrations by DSC

Fig. 6 Micrographs of CA and CN oleogels with different MY concentration. Scale bar 100X

Table 1. Fatty acids composition of the vegetable oils and monoglyceride

Fatty Acid	CA (%)	CN (%)	MY (%)
C6:0	-	$0.44{\pm}0.01$	-
C8:0	-	$6.59 {\pm} 0.12$	-
C9:0	-	$0.01 {\pm} 0.00$	-
C10:0	-	$5.28 {\pm} 0.00$	-
C11:0	-	$0.02 {\pm} 0.00$	-
C12:0	$0.01 {\pm} 0.00$	$46.23 {\pm} 0.37$	$0.19{\pm}0.00$
C14:0	$0.05 {\pm} 0.00$	$19.11 {\pm} 0.05$	$1.11 {\pm} 0.00$
C16:0	$3.95 {\pm} 0.06$	$10.21 {\pm} 0.11$	$58.72 {\pm} 0.10$
C16:1	$0.20 {\pm} 0.00$	$0.08 {\pm} 0.03$	-
C18:0	$1.52{\pm}0.01$	$2.87 {\pm} 0.04$	$39.67 {\pm} 0.11$
C18:1 cis	$65.15 {\pm} 0.05$	$7.52{\pm}0.09$	-
C18:2 cis	$19.53 {\pm} 0.15$	$1.58 {\pm} 0.02$	-
C18:3	$8.04 {\pm} 0.11$	-	-
C20:0	$0.41 {\pm} 0.00$	$0.06 {\pm} 0.00$	$0.31 {\pm} 0.00$
C20:1	$0.85 {\pm} 0.01$	-	
C20:2	$0.21 {\pm} 0.00$	-	
C20:3	$0.02{\pm}0.00$	-	
C24:1 cis	$0.08{\pm}0.00$	-	
ΣSFA	5.94	90.82	100
Σ MFA	66.28	7.60	0
ΣPFA	27.78	1.58	0
Σ Total	100	100	100

Saturated fatty acids (SFA), monounsaturated fatty acids (MFA), polyunsaturated fatty acids (PFA) **Table 2.** Temperatures and enthalpies of the MY obtained by DSC.

Crystallization profile

System	T_{CS} (°C)	T_{CO} (°C)	T_C (°C)	$\Delta H_{\rm C} (J/g)$
$\mathrm{CA}_{\mathrm{MGC}}$	36.43 ± 0.32^{a}	$35.16 {\pm} 0.06^{\rm a}$	$31.30 {\pm} 0.10^{\rm c}$	$1.41{\pm}0.08^{\rm a}$
CA_{SAT}	$49.06 \pm 0.08^{\circ}$	$48.96 {\pm} 0.14^{\rm c}$	$48.55 \pm 0.10^{\rm a}$	$9.81{\pm}1.68^{\rm b}$
$\mathrm{CN}_{\mathrm{MGC}}$	$37.28 {\pm} 0.03^{\rm b}$	$35.88 {\pm} 0.06^{\rm b}$	$28.96 {\pm} 0.19^{\rm b}$	$1.63{\pm}0.15^{\rm a}$
$\mathrm{CN}_{\mathrm{SAT}}$	$49.79 {\pm} 0.08^{\rm d}$	$49.66 {\pm} 0.08^{\rm d}$	$48.76 {\pm} 0.30^{\rm a}$	$8.41{\pm}1.34^{\rm b}$

Crystallization start temperatura (T_{CS}), crystallization onset temperatura (T_{CO}), crystallization temperatura (T_{C}), enthalpy of crystallization (ΔH_{C}), melting temperature (T_{M}), enthalpy of melting (ΔH_{M}). Comparison of means by column, different literals indicate significant difference

Table 3. Kinetic and thermal values of nucleation.

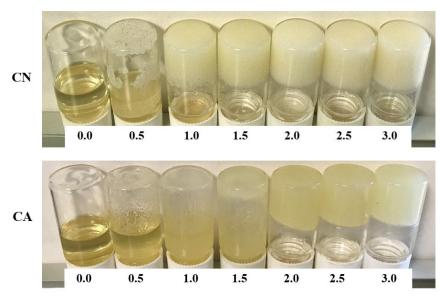
System	$t_n (min)$	J (min^{-1})	T_n (°C)	$[?]T_n$ (°C)	$\delta~(^{\circ}K/min)$	$[?]G_n (J/nucle)$
CA_{MGC}	$13.18 {\pm} 0.05^{\rm b}$	$0.08{\pm}0.00^{\rm b}$	$41.01 {\pm} 0.14^{\rm b}$	$38.99 {\pm} 0.14^{\rm b}$	$16.03 {\pm} 0.06^{\rm b}$	$-1.21E-26\pm7.91E-29^{\circ}$
CA_{SAT}	$10.25 {\pm} 0.12^{\rm a}$	$0.10{\pm}0.00^{\rm c}$	$49.57 \pm 0.35^{\circ}$	$30.43 {\pm} 0.35^{\mathrm{a}}$	$12.48{\pm}0.14^{\rm a}$	$-9.33E-27\pm1.41E-29^{b}$
$\mathrm{CN}_{\mathrm{MGC}}$	$13.80{\pm}0.20^{\circ}$	$0.07 {\pm} 0.00^{\mathrm{a}}$	$39.20{\pm}0.58^{\rm a}$	$40.81 {\pm} 0.58^{\circ}$	$16.78 {\pm} 0.24^{\circ}$	$-1.15E-26\pm 3.26E-28^{\circ}$
$\rm CN_{SAT}$	10.13 ± 0.12^{a}	$0.10{\pm}0.00^{\rm c}$	$49.89 \pm 0.35^{\circ}$	30.11 ± 0.35^{a}	12.35 ± 0.14^{a}	$-8.43E-27\pm2.28E-28^{a}$

Nucleation induction time (t_n) , nucleation rate (J), nucleation temperature (T_n) , conducting thermal force $([?]T_n)$, effective supercooling parameter (δ) , nucleation free energy $([?]G_n)$

Table 4. Parameters from Avrami model and Fractal dimension.

System	$z \pmod{1}$	n	\mathbf{R}^2	FD	\mathbf{R}^2
CA_{MGC}	$0.002 {\pm} 0.000$	$1.955{\pm}0.004$	0.96	1.95	0.99
$\mathrm{CA}_{\mathrm{SAT}}$	$0.029 {\pm} 0.000$	$0.961{\pm}0.006$	0.98	1.97	0.99
$\mathrm{CN}_{\mathrm{MGC}}$	$0.009 {\pm} 0.000$	$1.464{\pm}0.012$	0.95	1.96	0.99
$\mathrm{CN}_{\mathrm{SAT}}$	$0.033 {\pm} 0.002$	$0.807 {\pm} 0.024$	0.91	2.01	0.99

Growth rate (z), growth dimensionality (n), fractal dimension by correlation (FD_C)



MY concentration (% w/w)

